Articles

Dissection of Binding Interactions in the Complex between the Anti-Lysozyme Antibody HyHEL-63 and Its Antigen[†,‡]

Yili Li,[§] Mariela Urrutia,[§] Sandra J. Smith-Gill,[||] and Roy A. Mariuzza*[,§]

Center for Advanced Research in Biotechnology, W.M. Keck Laboratory for Structural Biology, University of Maryland Biotechnology Institute, 9600 Gudelsky Drive, Rockville, Maryland 20850, and National Cancer Institute, Frederick Cancer Research and Development Center, P.O. Box B, Frederick, Maryland 21702-1201

Received September 18, 2002

ABSTRACT: Alanine-scanning mutagenesis, X-ray crystallography, and double mutant cycles were used to characterize the interface between the anti-hen egg white lysozyme (HEL) antibody HyHEL-63 and HEL. Eleven HEL residues in contact with HyHEL-63 in the crystal structure of the antigen−antibody complex, and 10 HyHEL-63 residues in contact with HEL, were individually truncated to alanine in order to determine their relative contributions to complex stabilization. The residues of HEL (Tyr20, Lys96, and Lys97) most important for binding HyHEL-63 ($\Delta G_{mutant} - \Delta G_{wild\ type} > 3.0$ kcal/mol) form a contiguous patch at the center of the surface contacted by the antibody. Hot spot residues of the antibody ($\Delta\Delta G > 2.0$ kcal/mol) are organized in two clusters that juxtapose hot spot residues of HEL, resulting in energetic complementarity across the interface. All energetically critical residues are centrally located, shielded from solvent by peripheral residues that contribute significantly less to the binding free energy. Although HEL hot spot residues Lys96 and Lys97 make similar interactions with antibody in the HyHEL-63/HEL complex, alanine substitution of Lys96 results in a nearly 100-fold greater reduction in affinity than the corresponding mutation in Lys97. To understand the basis for this marked difference, we determined the crystal structures of the HyHEL-63/HEL Lys96Ala and HyHEL-63/HEL Lys97Ala complexes to 1.80 and 1.85 Å resolution, respectively. Whereas conformational changes in the proteins and differences in the solvent networks at the mutation sites appear too small to explain the observed affinity difference, superposition of free HEL in different crystal forms onto bound HEL in the wild type and mutant HyHEL-63/HEL complexes reveals that the side-chain conformation of Lys96 is very similar in the various structures, but that the Lys97 side chain displays considerable flexibility. Accordingly, a greater entropic penalty may be associated with quenching the mobility of the Lys97 than the Lys96 side chain upon complex formation, reducing binding. To further dissect the energetics of specific interactions in the HyHEL-63/HEL interface, double mutant cycles were constructed to measure the coupling of 13 amino acid pairs, 11 of which are in direct contact in the crystal structure. A large coupling energy, 3.0 kcal/mol, was found between HEL residue Lys97 and HyHEL-63 residue V_HAsp32, which form a buried salt bridge surrounded by polar residues of the antigen. Thus, in contrast to protein folding where buried salt bridges are generally destabilizing, salt bridges in protein−protein interfaces, whose residual composition is more hydrophilic than that of protein interiors, may contribute significantly to complex stabilization.

The ability of proteins to form specific, stable complexes with other proteins is fundamental to most cellular processes, including signal transduction, vesicle transport, and cytoskeletal remodeling. X-ray crystallographic studies of diverse protein−protein complexes (e.g., protease−protease inhibitor, antigen−antibody, hormone−hormone receptor, G-protein complexes) have revealed that most share a relatively large (>900 Å^2) and planar buried surface area composed of closely packed atoms, similar to protein cores (*1*−*7*). This shape complementarity is usually accompanied by a high degree of chemical complementarity. Hydrophobic patches on the surface of one protein pack against hydrophobic patches on the surface of the other protein, atoms of polar character interact with atoms of opposite charge across the interface, and proton donors and acceptors form hydrogen bonds. Protruding side chains of one surface fit into depressions of the other, and numerous van der Waals interactions are interspersed with hydrogen bonds and an oc-

[†] This work was supported by NIH Grant GM5280.

[‡] Atomic coordinates have been deposited in the Protein Data Bank as entries 1NBY and 1NBZ.

* To whom correspondence should be addressed. Tel.: 301-738-6243. FAX: 301-738-6255. E-mail: mariuzza@carb.nist.gov.

[§] University of Maryland Biotechnology Institute.

[||] Frederick Cancer Research and Development Center.

10.1021/bi020589+ CCC: $25.00
Published on Web 12/17/2002

casional salt bridge. Overall, protein−protein interfaces are quite polar and tend to reflect the residual composition of protein surfaces, rather than protein cores, although they are somewhat enriched in hydrophobic residues (*1*, *2*). Small, but significant, conformational changes are generally observed between free and bound proteins, and this flexibility appears to increase with the amount of buried surface area in the protein complex (*2*).

In contrast to the wealth of structural information on protein−protein interfaces, the available data on the thermodynamics of the association reactions are far more limited and are largely based on detailed mutagenesis and binding studies of relatively few complexes (*1*). These studies have shown that functional epitopes assigned by mutagenesis are usually, though not always (*7*−*10*), much more restricted than structural epitopes defined by X-ray crystallography (*1*, *5*, *6*, *11*). That is, replacement of only a small subset of contact residues ("hot spots") often destabilizes protein−protein complexes dramatically, while substitutions of most other interface residues, including many which appear to form highly favorable interactions, result in little or no loss of affinity. In other cases, however, the binding free energy arises from the accumulation of many productive interactions distributed over substantial portions of the interface (*7*−*10*, *12*). Indeed, a predictive understanding of protein−protein interactions has not been achieved and there is currently no method to reliably identify hot spot residues in complex structures based on patterns of shape, hydrophobicity or charge (*5*, *6*). A major difficulty is that interaction energies vary considerably, even for the same type of interaction, resulting in often poor correlations between structural data and energies deduced from mutagenesis. In addition, the relative contributions of surface complementarity, hydrophobicity, and hydrogen bonding to complex stabilization remain to be established. It is therefore evident that additional structure−function studies are required to progress from purely anatomical descriptions of protein−protein interfaces (identity of contact residues, amount of buried surface areas, number of hydrogen bonds and van der Waals interactions, etc.) to a detailed understanding of how these structural features translate to the affinity and specificity of binding reactions.

Antigen−antibody complexes provide useful models for analyzing the thermodynamics of protein−protein association reactions (*1*, *2*, *7*). We recently determined the crystal structure of the antigen-binding fragment (Fab) of the anti-hen egg white lysozyme (HEL) antibody HyHEL-63 complexed with HEL to 2.0 Å resolution, as well as structure of the unbound antibody in two crystal forms, to 1.8 and 2.1 Å resolution (*13*). The Fab HyHEL-63/HEL complex is highly suited for detailed structure−function studies of protein−protein recognition by mutational analysis: not only are the structures of both free and bound HyHEL-63 and HEL known to high resolution, but mutants of the antibody and antigen can be readily produced in bacteria and yeast, respectively. Furthermore, the affinities of mutant complexes can be accurately measured under equilibrium binding conditions using surface plasmon resonance (SPR) methods (*13*). Therefore, it should be possible to interpret the results of site-directed mutagenesis experiments in the HyHEL-63/HEL system in terms of the three-dimensional structures of the corresponding mutant complexes.

To assess the apparent contribution of individual residues to complex formation, we systematically truncated the side chains of contact residues on both HyHEL-63 and HEL to alanine and compared the affinities of the wild type and mutant complexes. We find that nearly all the contact residues tested (18 of 21) contribute at least 1.0 kcal/mol to the binding free energy. In common with most protein−protein complexes (*1*−*7*), energetically critical residues of HyHEL-63 and HEL are located at the center of the interface, surrounded by peripheral residues that contribute significantly less to complex stabilization. The two most energetically dominant HEL residues, Lys96 ($\Delta\Delta G = 6.1$ kcal/mol) and Lys97 (3.5 kcal/mol), form buried hydrogen bonds (Lys96) or a salt bridge (Lys97) in the wild-type complex. To explain the greater apparent contribution to binding of Lys96 than Lys97, we determined the crystal structures of the corresponding alanine-substituted complexes to high resolution. To further map the HyHEL-63/HEL interface, coupling energies between specific residue pairs were measured using double mutant cycles. Although the results were broadly consistent with expectations from structural analysis, we also encountered significant exceptions. Possible reasons for differences between actual and expected coupling energies for certain residue pairs are discussed in terms of the three-dimensional structure of the HyHEL-63/HEL complex.

EXPERIMENTAL PROCEDURES

Cloning and Mutagenesis of the HyHEL-63 Fab. The isolation of cDNAs for the L and H chains of anti-HEL antibody HyHEL-63 has been described (*13*). DNA fragments encoding the V_L and C_L domains of the L chain and the V_H and C_H1 domains of the H chain were generated by PCR and cloned downstream of the *pelB* leader sequence of expression vector pET-26b(+) (Novagen, Madison, WI). The vector was restricted with *Msc*I-*Sal*I and *Msc*I-*Hind*III for independent insertion of the V_LC_L and V_HC_H1 chains, respectively. The pET-26b(+)-V_HC_H1 construct was digested with *Xba*I, treated with Klenow large fragment (New England Biolabs, Beverly, MA) to generate blunt ends, and then restricted with *Not*I. The resulting fragment, containing the *pelB* leader and V_HC_H1, was cloned into pET-26b(+)-V_LC_L, which had been previously digested with *Sal*I, treated with Klenow large fragment, and restricted with *Not*I. In the final pET-26b(+)-V_LC_L/V_HC_H1 construct, the L and H chain genes are each fused to a *pelB* leader and controlled by the same T7 promoter. The V_HC_H1 gene also includes a sequence from the pET-26b(+) vector encoding a C-terminal His_6 tag for affinity purification. Site-directed mutagenesis of Fab HyHEL-63 was carried out by overlap PCR.

Production of Fab HyHEL-63 and Mutants by Secretion or in Vitro Folding. For protein expression, the pET-26b(+)-V_LC_L/V_HC_H1 plasmid was transformed into *Escherichia coli* strain BL21(D3) (Novagen). Precultures (3 mL) were grown at 37 °C overnight in Luria-Bertani (LB) medium containing 50 μg/mL kanamycin. These precultures were then

[1] Abbreviations: HEL, hen egg white lysozyme; PBS, phosphate-buffered saline; LB, Luria−Bertani medium; SPR, surface plasmon resonance; RU, resonance units; Fab, antigen-binding fragment; L chain, light chain; H chain, heavy chain; V region, variable region; C region, constant region; V_L, light chain variable region; V_H, heavy chain variable region; CDR, complementarity-determining region; FR, framework region.

used to inoculate 500 mL LB with the same antibiotic concentration. The bacteria were grown at 25 °C to an absorbance of 0.6−0.8 at 600 nm, and isopropyl β-D-thiogalactoside was added to a final concentration of 0.4 mM. After overnight incubation at 25 °C, the supernatant was separated from cells by centrifugation, concentrated using an Amicon RA2000 concentrator (Millipore, Bedford, MA), and buffer exchanged into 50 mM Tris-HCl, pH 8.0. The supernatant was applied to a Ni−NTA affinity column (QIAGEN, Valencia, CA) preequilibrated with the same buffer. The column was washed with 20 mM imidazole, 50 mM Tris−HCl, pH 8.0, and eluted with 50 mM imidazole, 50 mM Tris−HCl, pH 8.0. Fractions containing recombinant Fab HyHEL-63 were pooled, concentrated, and further purified by gel filtration on a Superdex S-200 FPLC column (Pharmacia, Uppsala, Sweden) to eliminate aggregates before surface plasmon resonance analysis (see below). Mutants of Fab HyHEL-63 were prepared similarly.

Wild-type Fab HyHEL-63 used for cocrystallization with HEL mutants Lys96gAla (HEL K96A) and Lys97gAla (HEL K97A) was produced by in vitro folding of the V_LC_L and V_HC_H1 chains, produced in *E. coli* as inclusion bodies, as described previously (*12*). Correctly folded protein was purified using an HEL affinity column, followed by anion exchange chromatography with a MonoQ FPLC column (Pharmacia).

Production of HEL Mutants. Mutants of HEL were produced as secreted proteins using an Invitrogen *Pichia* Expression Kit (San Diego, CA). A cDNA sequence encoding the wild-type protein fused to the leader sequence of α-mating factor was cloned into plasmid pPic9 as a *Xho*I/*Not*I fragment (*14*). Mutagenesis was carried out by overlap PCR. For protein production, yeast from a single colony transformed with this plasmid was grown in 25 mL BMGY medium at 28−30 °C. After the culture reached an absorbance of 1.0−6.0 at 600 nm, the cells were harvested by centrifugation at 1500*g*; the pellets were suspended in BMMY medium to an absorbance of 1.0 prior to induction. Methanol was added to the culture every 24 h to a final concentration of 0.5% (v/v) to maintain induction. After 96 h, the culture was harvested by centrifugation. The supernatant was dialyzed overnight against 0.1 M ammonium acetate, pH 9.0, and loaded on a 3 mL CM-Sepharose Fast Flow column (Pharmacia) previously equilibrated with the same buffer. The column was washed with 10 volumes of buffer and eluted with 0.5 M ammonium acetate, pH 9.0. Further purification was carried out on a Mono S cation exchange FPLC column (Pharmacia) equilibrated with 50 mM MES, pH 6.5, and developed with a linear NaCl gradient; all HEL mutants eluted between 0.2 and 0.4 M NaCl.

Affinity Measurements. The interaction of soluble Fab HyHEL-63 with immobilized HEL was measured by SPR using a BIAcore 1000 biosensor (BIACORE, Piscataway, NJ) as described (*8*, *15*, *16*). The data were analyzed using the BIAevaluation 2.1 software package (BIACORE). Association constants (K_As) were determined from Scatchard analysis, after correction for nonspecific binding, by measuring the concentration of free reactants and complex at equilibrium. Standard deviations for two or more independent K_A determinations were typically <20%.

Crystallography. The Fab HyHEL-63/HEL K96A and Fab HyHEL-63/HEL K97A complexes were crystallized at room temperature in hanging drops from mixtures containing equimolar amounts of antibody and antigen at 10 mg/mL concentrations. The crystallization conditions were similar to those for the wild-type Fab HyHEL-63/HEL complex (*13*): 15% (w/v) PEG 4000, 0.1 M ammonium acetate, and 0.05 M sodium acetate, pH 4.6. The mutant complexes crystallized isomorphously with the wild-type in space group $P4_22_12$ with one complex molecule per asymmetric unit (Table 1). X-ray diffraction data were measured at 100 K on beamline 19-ID ($\lambda = 0.978$ Å) of the Advanced Photon Source (Argonne National Laboratory) using an ADSC Quantum-4 CCD detector. The crystals were transferred to a cryoprotectant solution (mother liquor containing 25% glycerol), prior to flash-cooling in a nitrogen stream. The data were processed and scaled using DENZO/SCALEPACK (*17*), followed by data reduction using programs from the CCP4 suite (*18*). Data collection statistics are shown in Table 1.

Table 1: Data Collection and Refinement Statistics for HyHEL-63/HEL Complexes

	HyHEL-63/HEL K96A	HyHEL-63/HEL K97A
Data Collection		
space group	$P4_22_12$	$P4_22_12$
cell dimensions(Å)	$a = b = 90.9$, $c = 151.9$	$a = b = 90.9$, $c = 151.2$
temperature (K)	100	100
resolution limit (Å)	1.80	1.85
mosaicity (Å)	0.3	0.4
R_{merge} (%)[b]	5.9 (42.2)[a]	5.4 (36.6)[a]
unique reflections	114 251	53 340
total observations	430 270	472 861
completeness (%)	99.9 (100)[a]	97.3 (93.2)[a]
Refinement		
R_{free}[c]	24.2	24.5
R_{cryst}	20.1	18.5
protein		
residues	553	553
average B (Å^2)	21.4	21.7
water		
molecules	743	608
average B (Å^2)	36.1	35.7
rms deviations		
bonds (Å)	0.017	0.006
angles (deg)	0.024	0.022

[a] Values in parentheses correspond to the highest resolution shell: HyHEL-63/HEL K96A (1.86−1.80 Å); HyHEL-63/HEL K97A (1.92−1.85 Å). [b] $R_{merge} = \sum|I - \langle I\rangle|/\sum\langle I\rangle$, where I is the observed intensity and $\langle I\rangle$ is the average intensity of multiple observations of symmetry-related reflections. [c] A portion of the overall reflections was set aside for R_{free} calculations: HyHEL-63/HEL K96A (9.7%); HyHEL-63/HEL K97A (9.6%).

The structures of the Fab HyHEL-63/HEL K96A and Fab HyHEL-63/HEL K97A complexes were solved by molecular replacement methods using the program AMoRe (*19*), with the wild-type complex (PDB accession code 1DQM) (*12*) as a search model. Crystallographic refinement was carried out using X-PLOR3.1 (*20*) and CNS0.4 (*21*), including rigid-body refinement, iterative cycles of simulated annealing, positional refinement, torsion angle refinement, and individual temperature factor (B) refinement interspersed with manual model fitting into σ_A-weighted F_o-F_c and $2F_o-F_c$ electron density maps using TURBO−FRODO (*22*). Water molecules were added at positions where the F_o-F_c electron density was greater than 2.5σ and where reasonable hydrogen bonds to protein atoms or other water molecules were

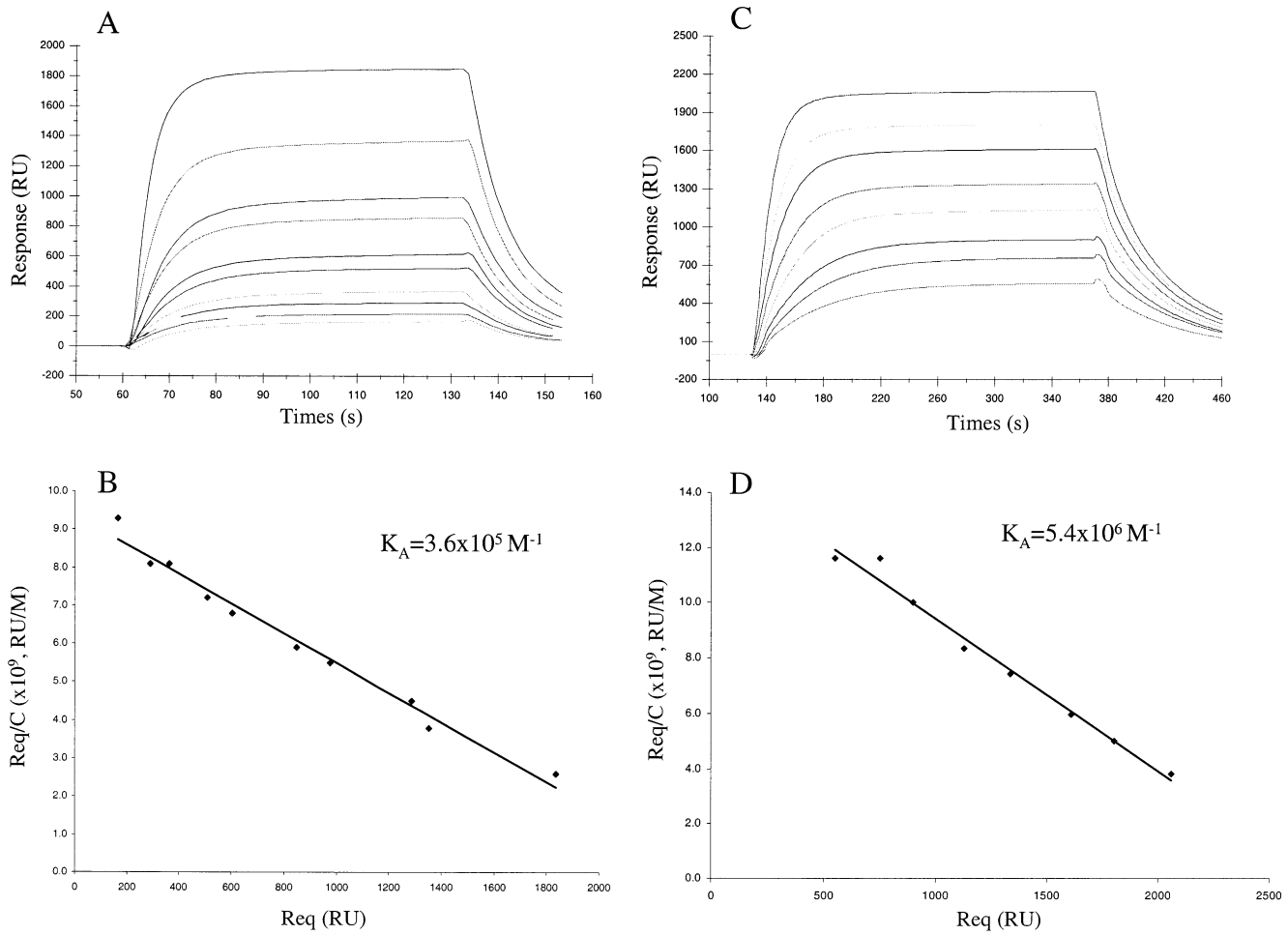

FIGURE 1: (A) Binding of Fab HyHEL-63 V_LN32A to immobilized wild-type HEL. The HyHEL-63 mutant was injected at 10 different concentrations ranging from 0.2 to 7.1 μM over a surface to which 1200 RU of wild-type HEL had been coupled. Buffer flow rates were 5 μL/min, and report points were taken 1 min after each injection. (B) Scatchard plot of the binding of Fab HyHEL-63 V_LN32A to wild-type HEL derived from the data depicted in panel A after correction for nonspecific binding; R_{eq} is the corrected equilibrium response at a given concentration *C*. The plot is linear with a correlation coefficient of 0.98. The apparent K_A is 3.6×10^5 M^{-1}. The predicted maximum binding capacity (4100 RU) indicates that about 59% of the immobilized wild-type HEL molecules are available for binding. (C) Binding of Fab HyHEL-63 V_HD32A to immobilized HEL K97A. The HyHEL-63 mutant was injected at eight different concentrations ranging from 42 to 540 nM over a surface to which 1400 RU of the HEL mutant had been coupled. Report points were taken 3.5 min after each injection. (D) Scatchard plot derived from the data in panel C after correction for nonspecific binding. The plot is linear with a correlation coefficient of 0.98 and the apparent K_A is 5.4×10^6 M^{-1}. Approximately 56% of the immobilized HEL K97A is available for binding, as calculated from the predicted maximum binding capacity (4800 RU).

possible. The final Fab HyHEL-63/HEL K96A structure, determined to 1.80 Å resolution, has an R_{cryst} of 19.7% and an R_{free} of 24.0%. For the Fab HyHEL-63/HEL K97A complex, the final R_{cryst} is 19.7% and R_{free} is 25.0% at 1.85 Å resolution. The Fab HyHEL-63/HEL K96A and Fab HyHEL-63/HEL K97A models include 743 and 608 water molecules, respectively. Refinement statistics are summarized in Table 1.

RESULTS AND DISCUSSION

Production of Recombinant Fab HyHEL-63. Because of its nonreducing environment, the periplasmic space of *E. coli* has been used for the expression of heterologous proteins, such as antibodies (*8*, *23*, *24*) and T-cell receptors (*25*, *26*), that contain disulfide bonds. To direct secretion of Fab HyHEL-63 into the periplasmic space, the natural signal sequences of its L and H chains were replaced with that of pectate lyase from *Erwinia carotovora* (*23*, *24*). Six histidine-encoding triplets were grafted onto the 3′ terminus of the V_HC_H1 gene to permit purification of the recombinant protein using a nickel chelate adsorbent. This was done to avoid HEL affinity chromatography, since certain HyHEL-63 mutants were expected to bind the antigen too weakly for purification by this method. Surprisingly, most of the antibody was found in the culture supernatant, rather than the periplasmic space, indicating leakage from the periplasmic compartment due to membrane damage or cell lysis, as occasionally observed for secreted antibodies (*8*, *16*, *23*, *24*).

In our previous crystallographic study of the Fab HyHEL-63/HEL complex, we had expressed the wild-type Fab by in vitro folding of the V_LC_L and V_HC_H1 chains, produced as bacterial inclusion bodies (*12*). Since secreted Fab HyHEL-63 did not crystallize with HEL under wild-type conditions, perhaps due to the presence of a flexible His_6 tag, the Fab used for crystallizing complexes with HEL mutants was produced by in vitro folding. Importantly, the affinities of the secreted and in vitro folded forms of HyHEL-63 for HEL were indistinguishable (data not shown).

Measurement of Association Constants for the Binding of HyHEL-63 to HEL. The affinities of wild-type and mutant

HyHEL-63 Fab fragments for wild-type HEL or HEL mutants were determined under equilibrium binding conditions with a BIAcore biosensor. Typically, analyte concentrations ranging from 1/10 the dissociation constant (K_D) to 10K_D were used; higher concentrations were required to approach saturation for the lower affinity interactions. Surface plasmon resonance profiles for equilibrium binding of HyHEL-63 mutant V_LN32A mutant to immobilized wild-type HEL, and of HyHEL-63 mutant V_HD32A to HEL mutant K97A, are shown in Figure 1 (panels A and C, respectively). The corresponding Scatchard plots, after correcting for nonspecific binding, are shown in Figure 1 (panels B and D). The plots were linear, and apparent K_As were calculated as the slopes of the straight lines: $K_A = 3.6 \times 10^5$ M^{-1} and 5.4×10^6 M^{-1} for the HyHEL-63 V_LN32A/HEL and HyHEL-63 V_HD32A/HEL K97A interactions, respectively. The predicted maximum specific binding, calculated from the *x*-intercept assuming a linear relationship between the mass of bound protein and the measured resonance units (RU) (*26*), indicated that approximately 60% of the immobilized HEL molecules were available for binding in both cases. The affinities measured by equilibrium binding were very reproducible, and deviations between different runs on the same chip were generally smaller than those between different chips. The errors on K_A were consistently less than 20%, which translates into errors on $\Delta\Delta G$ ($\Delta G_{mutant} - \Delta G_{wild\ type}$) and $\Delta\Delta G_{int}$ (the interaction energy between residue pairs from double mutant cycle analysis) of less than ±0.4 and ±0.7 kcal/mol, respectively. Thus, the binding of closely related mutant proteins may be compared with a relatively high degree of precision using this BIAcore method.

Mapping the Energetics of the HyHEL-63/HEL Interface. Residues in the interface between HyHEL-63 and HEL were subjected to alanine-scanning mutagenesis in order to determine their relative contributions to the free energy of association. In the crystal structure of the Fab HyHEL-63/HEL complex (*13*), 19 HyHEL-63 residues from all six complementarity-determining regions (CDRs) of the antibody, and 1 H chain framework region residue, contact 20 HEL residues from three discontinuous polypeptide segments of the antigen. We individually mutated to alanine 11 HEL residues in contact with HyHEL-63, excluding 2 glycine residues (16 and 102) and residues contacting the antibody only through backbone atoms (14, 15, 18, 19, and 98). The binding affinities of these HEL mutants for wild-type HyHEL-63 were measured by BIAcore and $\Delta\Delta G$s calculated (Table 2, section A). The most destabilizing mutation was at position Lys96 ($\Delta\Delta G = 6.1$ kcal/mol). In the wild-type structure, this residue makes two hydrogen bonds to V_LAsn31 and V_LAsn32 ($Lys96_{HEL}$ Nζ−Oδ1 V_LAsn31 and $Lys96_{HEL}$ Nζ−Oδ1 V_LAsn32). Alanine substitutions at HEL positions Tyr20 and Lys97 also greatly reduced binding ($\Delta\Delta G > 3.0$ kcal/mol). Smaller, but significant, effects were observed for substitutions at positions Arg21, Trp63, Leu75, and Asp101 (1.0−2.0 kcal/mol), while those at positions Trp62, Thr89, Asn93, and Ser100 had very little effect (<1.0 kcal/mol). These results are broadly consistent with those from a mutational study of the anti-HEL antibody HyHEL-10 (*28*), which recognizes a similar epitope on HEL as HyHEL-63 (*13*, *29*).

Table 2: Association Constants and Relative Free-Energy Changes for Single and Double Mutant Complexes[a]

HyHEL-63 wt	HEL	K_A (M^{-1}) $(3.6 \pm 0.1) \times 10^8$	$\Delta\Delta G$ (kcal/mol)
		Section A	
wt	Y20A	$(1.4 \pm 0.2) \times 10^6$	3.3
wt	R21A	$(4.3 \pm 0.4) \times 10^7$	1.3
wt	W62A	$(1.0 \pm 0.1) \times 10^8$	0.8
wt	W63A	$(3.7 \pm 0.2) \times 10^7$	1.3
wt	L75A	$(3.1 \pm 0.2) \times 10^7$	1.5
wt	T89A	$(8.7 \pm 2.3) \times 10^7$	0.8
wt	N93A	$(1.2 \pm 0.3) \times 10^8$	0.6
wt	K96A	$(1.1 \pm 0.3) \times 10^4$	6.1
wt	K97A	$(9.4 \pm 1.0) \times 10^5$	3.5
wt	S100A	$(9.7 \pm 0.5) \times 10^7$	0.8
wt	D101A	$(4.0 \pm 0.8) \times 10^7$	1.3
		Section B	
V_LN31A	wt	$(1.2 \pm 0.1) \times 10^7$	2.0
V_LN32A	wt	$(3.6 \pm 0.2) \times 10^5$	4.1
V_LY50A	wt	$(3.9 \pm 0.2) \times 10^6$	2.7
V_LS91A	wt	$(3.2 \pm 0.1) \times 10^7$	1.4
V_LY96A	wt	$(5.3 \pm 0.1) \times 10^7$	1.1
V_HD32A	wt	$(1.2 \pm 0.2) \times 10^7$	2.0
V_HY33A	wt	$(3.2 \pm 0.1) \times 10^4$	5.5
V_HY50A	wt	$(3.2 \pm 0.8) \times 10^3$	6.9
V_HY53A	wt	$(4.9 \pm 0.7) \times 10^7$	1.2
V_HW98A	wt	$(8.7 \pm 1.2) \times 10^4$	4.9
		Section C	
V_LN32A	K96A	$(2.0 \pm 0.2) \times 10^4$	5.8
V_LS91A	R21A	$(1.7 \pm 0.1) \times 10^6$	3.2
V_LS91A	Y20A	$(8.6 \pm 2.0) \times 10^5$	3.6
V_LY96A	R21A	$(1.0 \pm 0.2) \times 10^6$	3.5
Y_LY96A	S100A	$(7.7 \pm 0.3) \times 10^7$	0.9
Y_HD32A	K97A	$(5.4 \pm 0.4) \times 10^7$	2.5
V_HY53A	W62A	$(4.1 \pm 0.5) \times 10^7$	1.3
V_HY53A	W63A	$(8.8 \pm 1.0) \times 10^6$	2.2
V_HY53A	L75A	$(4.6 \pm 0.5) \times 10^7$	1.2
V_HY53A	D101A	$(3.6 \pm 0.5) \times 10^6$	2.7
V_HW98A	S100A	$(4.2 \pm 0.8) \times 10^4$	5.3
V_HW98A	K97A	$(4.7 \pm 1.0) \times 10^3$	6.6
V_HW98A	Y20A	$(6.4 \pm 0.7) \times 10^4$	5.1

[a] Affinity measurements were carried out by BIAcore as described in Experimental Procedures. Wt refers to wild-type protein. Differences in free energy changes are calculated as the difference between the ΔGs of the mutant wild-type reactions ($\Delta\Delta G = \Delta G_{mutant} - \Delta G_{wild-type}$). Sections A and B show affinities and $\Delta\Delta G$s for single mutants of HyHEL-63 and HEL, respectively. Sections C shows values for the double mutants.

On the antibody side of the interface, 10 HyHEL-63 residues (5 from V_L and 5 from V_H) in contact with HEL were mutated to alanine. The affinities of these mutants for wild-type HEL are shown in Table 2, section B. Overall, mutations in the H chain disrupt binding more than those in the L chain. Three H chain mutations, at position V_HTyr33, V_HTyr50 and V_HTrp98, are associated with $\Delta\Delta G$ values exceeding 4.0 kcal/mol. The corresponding residues of HyHEL-10 are also hot spots for HEL binding (*30*). Two L chain mutations, at positions V_LAsn32 and V_LTyr50, also significantly reduced binding, with $\Delta\Delta G$s of 4.1 and 2.7 kcal/mol, respectively. Substitutions at the other five antibody positions tested (V_LAsn31, V_LSer91, V_LTyr96, V_HAsp32, and V_HTyr53) had less effect (1.1−2.0 kcal/mol). In the HyHEL-10/HEL complex, mutation of the conserved V_LAsn31 residue results in a much greater affinity loss ($\Delta\Delta G = 5.2$ kcal/mol), possibly reflecting the longer distance of the conserved hydrogen bond to $Lys96_{HEL}$ in the HyHEL-63/HEL complex and the fewer number of van der Waals contacts made with the antigen (*13*).

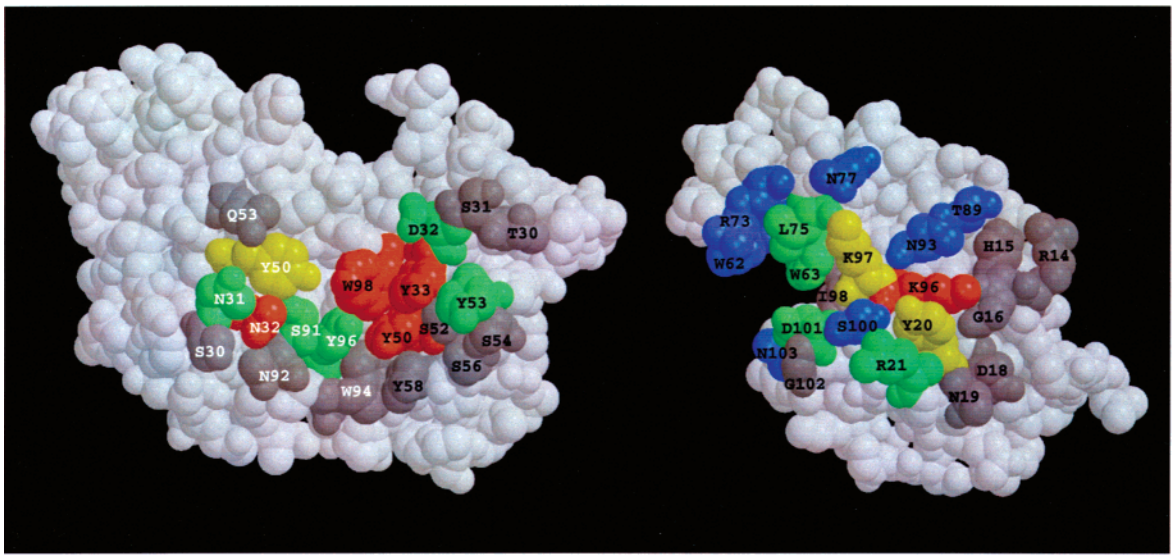

FIGURE 2: Space-filling model of the surface of HyHEL-63 (left) in contact with HEL and of the surface of HEL (right) in contact with HyHEL-63. The two proteins are oriented such that they can be docked by folding the page along a vertical axis between the components. Residues are color-coded according to the loss of binding free energy upon alanine substitution: red, >4 kcal/mol; yellow, 2−4 kcal/mol; green, 1−2 kcal/mol; blue, <1 kcal/mol. In dark gray are contacting residues in the HyHEL-63/HEL interface that were not tested by alanine-scanning mutagenesis. V_L residues are labeled in white and V_H residues in black.

Figure 2 shows the residues of HyHEL-63 and HEL important in complex stabilization mapped onto the three-dimensional structure of each protein. The residues of HEL most important for binding HyHEL-63 (Tyr20, Lys96 and Lys97) form a contiguous patch located at the center of the surface contacted by the antibody. The three hot spot residues ($\Delta\Delta G$ > 2.0 kcal/mol) of the HyHEL-63 H chain (V_HTyr33, V_HTyr50 and V_HTrp98) cluster together, as do the two hot spot residues of the L chain (V_LAsn32 and V_LTyr50), forming two energetically important patches on the antibody surface. A comparison of the interacting surfaces in Figure 2 reveals that hot spot residues on the HEL side of the interface generally correspond to hot spots on the HyHEL-63 side. For example, in the crystal structure of the complex (*13*), hot spot residue $Lys97_{HEL}$ ($\Delta\Delta G$ = 3.5 kcal/mol) makes contact with hot spot residues V_HTyr33 (5.5 kcal/mol) and V_HTrp98 (4.9 kcal/mol). Similarly, hot spot residues $Tyr20_{HEL}$ (3.3 kcal/mol) and $Lys96_{HEL}$ (6.1 kcal/mol) contact hot spot residues V_LAsn32 (4.1 kcal/mol) and V_LTyr50 (2.7 kcal/mol). In addition, functionally less important residues of HyHEL-63 and HEL tend to be juxtaposed in the antigen−antibody interface: V_HTyr53 ($\Delta\Delta G$ = 1.2 kcal/mol) interacts with HEL residues Trp63, Leu75 and Asp101 (1.0−2.0 kcal/mol), while V_LTyr96 (1.1 kcal/mol) contacts HEL residues Arg21 (1.3 kcal/mol) and Ser100 (0.8 kcal/mol). A significant exception to this energetic complementarity is V_HTyr50, whose replacement by alanine results in a decrease in binding free energy of 6.9 kcal/mol, the largest for any residue tested, but which interacts with functionally far less important HEL residues Arg21 and Ser100 (Table 2). One possible explanation for this discrepancy is that the V_HTyr50 side chain contacts Ser100 only through main-chain atoms, such that the relative contribution of the HEL residue cannot be assessed by simple alanine substitution. In addition, the side chain of V_HTyr50 is mostly buried in the antibody combining site: the solvent-accessible surface area of this residue is only 24 Å^2, compared to 77 Å^2 for V_HTyr33, 153 Å^2 for V_HTyr53, and 100 Å^2 for V_HTyr58. Thus, the large decrease in affinity upon replacement of V_HTyr50 by alanine may be an indirect effect due to structural perturbations in the antibody combining site propagating from the mutation to neighboring residues, in particular V_HTyr58, V_HTrp98, V_LTrp94, and V_LTyr96, which make numerous contacts with HEL. If so, V_HTyr50 may not represent a true hot spot for HEL binding; similar considerations may apply to certain hot spots in other protein−protein interfaces identified by alanine-scanning mutagenesis (*6*). Overall, however, these results are in agreement with findings from other antigen−antibody systems (*1*, *7*), and the growth hormone-growth hormone receptor complex (*11*, *31*−*33*), that energetically critical residues tend to be self-complementary across interfaces.

As noted for several other protein−protein complexes (*1*, *8*, *11*, *34*), the change in solvent-accessible surface area of individual HyHEL-63 or HEL residues upon complex formation does not correlate well with their relative importance to binding. For example, V_HTyr53 and $Arg21_{HEL}$ contribute the most to the buried surface in the HyHEL-63−HEL interface (111 Å^2 and 116 Å^2, respectively), yet are not hot spot residues (Table 2). A far more important parameter in determining a particular residue's contribution to complex stabilization appears to be its location in the interface (central versus peripheral), although the reasons for this marked positional dependence are incompletely understood (see Conclusions) (*1*, *6*). Thus, hot spot residues such as V_HTyr33 and V_HTrp98 of HyHEL-63, or Tyr20 and Lys96 of HEL, are located near the center of the interface, where they are mostly shielded from bulk solvent (>70% burial) by peripheral residues that contribute significantly less to the binding free energy (Figure 2).

Structures of HEL Mutants K96A and K97A Complexed with HyHEL-63. In the wild-type HyHEL-63/HEL complex, the interacting surface of HyHEL-63 is mainly hydrophobic, whereas hydrophilic residues predominate on the HEL side of the interface (*13*). Of the three hot spot HEL residues we identified, two (Lys96 and Lys97) are charged. In the crystal structure, the aliphatic portion of the $Lys96_{HEL}$ side chain

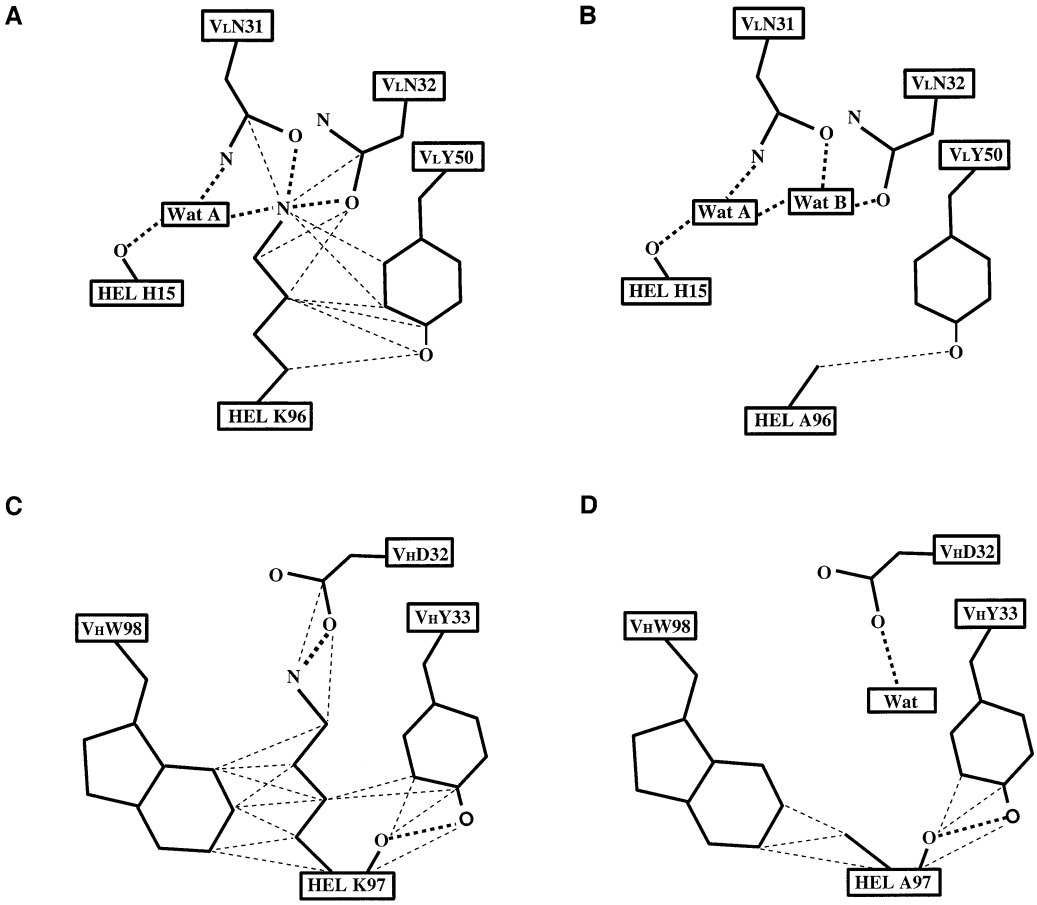

FIGURE 3: (A) Schematic representation of the wild-type Fab HyHEL-63/HEL complex in the vicinity of HEL residue Lys96. Hydrogen bonding interactions are represented by thick dotted lines; van der Waals contacts are drawn as thin dotted lines. (B) Schematic showing the same region in the HyHEL-63/HEL K96A mutant complex. Wat A is a water molecule present in both wild-type and mutant structures; Wat B is an additional water in the HyHEL-63/HEL K96A interface. (C) Schematic of the wild-type Fab HyHEL-63/HEL complex in the vicinity of HEL residue Lys96. (D) Schematic showing the same region in the HyHEL-63/HEL K97A mutant complex. A water (Wat) partially fills the cavity formed by truncation of the lysine side chain.

packs against the aromatic ring of V_LTyr50, while the charged Nζ group is neutralized by hydrogen bonding to the Oδ1 groups of V_LAsn31 and V_LAsn32 (Figure 3A). Similarly, the side chain of $Lys97_{HEL}$ intercalates between aromatic residues V_HTyr33 and V_HTrp98, with the Nζ group neutralized by a salt bridge to V_HAsp32 (Figure 3C). The affinity of HEL K96A for HyHEL-63 ($K_A = 1.1 \times 10^4$ M^{-1}) is approximately 33 000-fold lower than that of wild-type HEL (3.6×10^8 M^{-1}), while the affinity of HEL K97A (9.4×10^5 M^{-1}) is only 380-fold lower (Table 2).

To understand how replacement of these two charged residues by alanine disrupts binding and why mutation of $Lys96_{HEL}$ results in a nearly 100-fold greater reduction in affinity than mutation of $Lys97_{HEL}$, we determined the crystal structures of the HyHEL-63/HEL K96A and HyHEL-63/HEL K97A complexes to 1.80 and 1.85 Å resolution, respectively. Omit maps in the region of the mutations are shown in Figure 4A,C. The root-mean-square (rms) deviations in α-carbon positions between mutant and wild-type structures are only 0.27 Å for HyHEL-63/HEL K96A and 0.34 Å for HyHEL-63/HEL K97A, indicating that the mutations do not significantly alter the overall structure of the complexes. Conformational changes in the proteins at the mutation sites are also small (Figure 4B,D).

The principal difference in the structure of the mutant complexes is a rearrangement of solvent such that additional water molecules are stably incorporated in the interface at the site of the mutations. In the HyHEL-63/HEL K96A complex, the cavity created by the alanine substitution is partially filled by a water molecule (WatB) that forms hydrogen bonds which mimic ones made by $Lys96_{HEL}$ (Figure 3B). In the wild-type structure, WatA, which is also present in the mutant complex, forms hydrogen bonds with $His15_{HEL}$ O, $Lys96_{HEL}$ Nζ, and V_LAsn31 Nδ2 (Figure 3A). In the mutant, WatB fulfills the role of $Lys96_{HEL}$ by hydrogen bonding to V_LAsn31, V_LAsn32, and WatA. However, nearly all direct interactions between the $Lys96_{HEL}$ side chain and HyHEL-63 are lost when this residue is mutated to alanine, including nine van der Waals contacts and two hydrogen bonds, which are not replaced by newly formed water-mediated interactions. A similar situation exists for the HyHEL-63/HEL K97A complex, where a water molecule occupies only part of the cavity created by the side-chain truncation, hydrogen bonding to V_HAsp32 Oδ2 (Figure 3D). Nine van der Waals contacts and one salt bridge ($Lys97_{HEL}$ Nζ−Oδ2 V_HAsp32) are lost in the mutant complex, none of which are restored by the sole additional water molecule at the mutation site. For both complexes, the observed solvent rearrangements are clearly insufficient to compensate for the loss of direct protein−protein interactions at the mutation sites, thereby contributing to the large reductions in binding affinity relative to the wild-type complex. Moreover, differ-

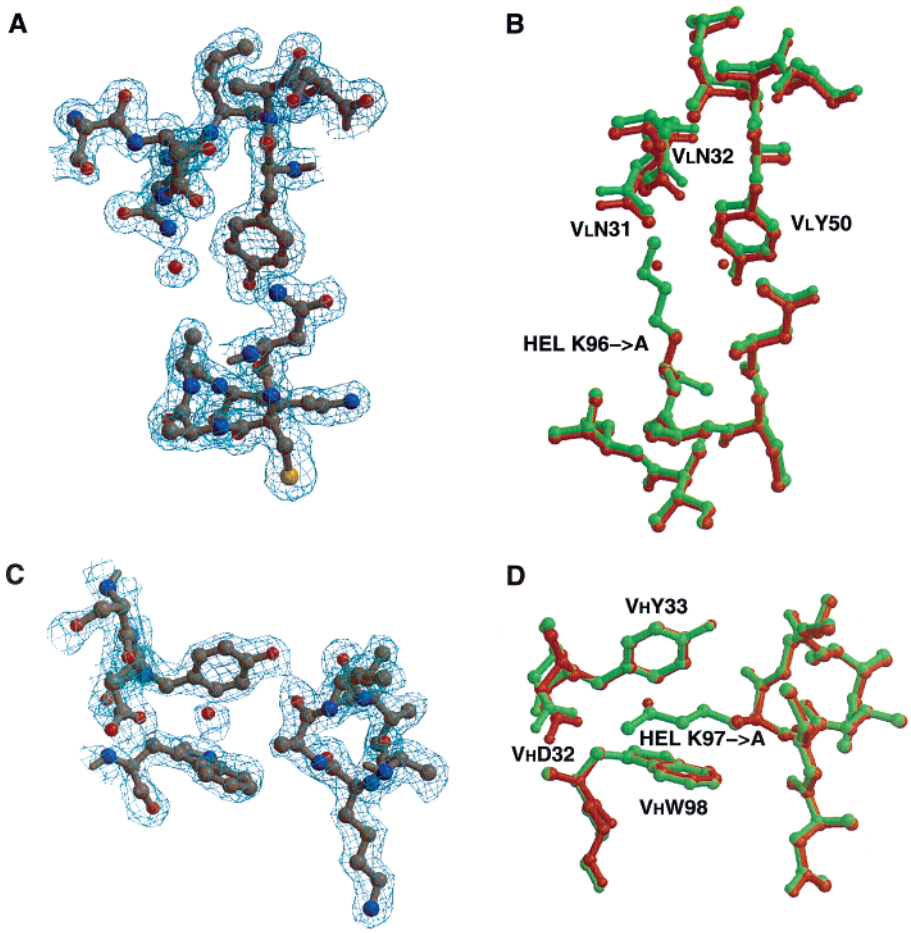

FIGURE 4: (A) Simulated annealing omit electron density map in the vicinity of HEL residue Ala96 in the HyHEL-63/HEL K96A mutant complex. The map was calculated using CNS0.4 (*21*), where all atoms within a 9 Å radius of $Ala96_{HEL}$ were omitted from the calculation. Contours are at 1σ. (B) Superposition of the HyHEL-63/HEL K96A mutant complex (red) onto the wild-type structure (green). The view is the same as in panel A. (C) Simulated annealing omit map in the region of HEL residue Ala97 in the HyHEL-63/HEL K97A mutant complex. (D) Superposition of the HyHEL-63/HEL K97A mutant complex (red) onto the wild-type structure (green).

ences in the nature or extent of the solvent networks formed in the mutant complexes (Figure 3B,D) appear too limited to explain the much greater effect on binding of alanine substitution of $Lys96_{HEL}$ than $Lys97_{HEL}$ (Table 2).

We had previously observed solvent rearrangements, including the incorporation of additional interface waters, in X-ray crystallographic studies of complexes between site-directed mutants of the anti-HEL antibody D1.3 and HEL (*16*, *35*, *36*). In certain cases, the mutations were associated with only small reductions in affinity (<10-fold), even though they resulted in the loss of a similar number of van der Waals and hydrogen bond interactions as in the HyHEL-63/HEL K96A and HyHEL-63/HEL K97A complexes (*16*, *35*). In other cases, up to 1000-fold reductions in affinity were observed (*35*, *36*). Even more drastic is the 33 000-fold loss of affinity measured in the present study for the HyHEL-63/HEL K96A interaction. Thus, there appears to be a very wide range in the extent to which solvent rearrangements in a protein−protein interface can accommodate mutations, which probably depends on the position of the mutation in the interface and on the nature of the local environment. On the basis of the available crystal structures (*16*, *35*−*38*), we conclude that sites at the periphery of protein−protein interfaces, because of their accessibility, are particularly suited to the incorporation of new waters to occupy cavities or channels created by side-chain truncations, provided that the local environment is sufficiently polar to permit the formation of a stable water network to compensate the loss of complementarity at the mutation site. For example, alanine substitution of D1.3 residue V_HTpr52 has little effect on HEL binding, whereas V_HTrp92 is a hot spot, even though both tryptophans are near the periphery of the D1.3-HEL interface and make similar contributions to the buried surface in the complex (*8*). However, examination of the atomic interactions made by these residues reveals that V_HTrp92 packs against a more hydrophobic surface than V_HTrp52, precluding the formation of compensating water-mediated interactions with HEL (*36*). We also fail to observe such interactions for residues at the center of interfaces, such as $Lys96_{HEL}$ and $Lys97_{HEL}$ in the HyHEL-63/HEL complex (Figure 3B,D), which are buried in predominantly hydrophobic environments.

A possible explanation for the much greater apparent contribution to binding of $Lys96_{HEL}$ ($\Delta\Delta G = 6.1$ kcal/mol) than $Lys97_{HEL}$ (3.5 kcal/mol) may be found by comparing the conformations of these residues in different crystal packing environments. Superposition of free HEL in three crystal forms (*39*−*41*) onto bound HEL in the HyHEL-63/HEL complex (*13*) shows that the side chain conformations of $Lys96_{HEL}$ are very similar in the four structures, whereas the $Lys97_{HEL}$ side chain displays considerable conformational variability (Figure 5A). Thus, a significant entropic penalty

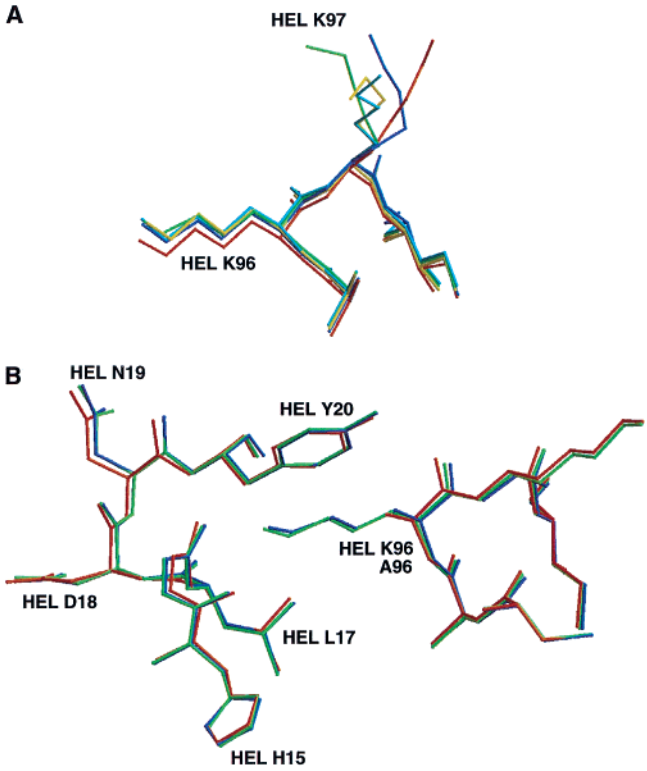

FIGURE 5: (A) Conformational differences in HEL residues Lys96 and Lys97. Complexed HEL (red) was superposed onto four crystal forms of free HEL (monoclinic, green; orthorhombic, cyan; tetragonal, yellow; trigonal, blue). (B) Displacement of HEL residues 15−20 in the HyHEL-63/HEL K96A mutant complex (red) compared to the wild-type (green) and HEL K97A mutant (blue) complexes.

may be associated with quenching the mobility of the flexible $Lys97_{HEL}$ side chain upon complex formation, which would be unfavorable for binding. This penalty should be less for the $Lys96_{HEL}$ side chain, whose conformation in the bound state is nearly identical to those found in different crystal forms of the free antigen (*39*−*41*). Another factor contributing to the greater decrease in affinity upon mutation of $Lys96_{HEL}$ could be that this residue is more deeply buried in the HEL structure than $Lys97_{HEL}$: the solvent-accessible surface area of $Lys96_{HEL}$ is only 35 Å^2 compared to 102 Å^2 for $Lys97_{HEL}$. Alanine substitution of $Lys96_{HEL}$ may therefore result in rearrangements of neighboring HEL residues, reducing interface complementarity at the mutation site. Indeed, a comparison of the wild-type and mutant HyHEL-63/HEL structures reveals a small, but significant, displacement (up to 0.4 Å) in the position of the peptide backbone of HEL residues 15−20 in the HEL K96A mutant complex, relative to wild-type, that is not observed in the HEL K97A complex (Figure 5B).

Analysis of the HyHEL-63/HEL Interface Using Double Mutant Cycles. Comparing the binding of a wild-type protein with that of a mutant in which a side chain has been truncated gives an apparent binding energy which is generally greater than the incremental binding energy attributable to that side chain (*42*), since interactions other than the interactions of interest are often disrupted, each of which may contribute to the energetics of association (*43*−*45*). These secondary effects include possible conformational changes in the proteins ranging from repositioning of side chains to movements in the backbone, as well as reorganizations in solvent structure in the vicinity of the mutation. Such effects are evident in the crystal structures of the HyHEL-63/HEL K96A and HyHEL-63/HEL K97A complexes described above, although they are of relatively moderate magnitude for both mutants.

The method of double mutant cycles circumvents many of the limitations of single mutant experiments and makes it possible to estimate the effective interaction energy between specific residues in a protein−protein complex independently of interactions other than those between the residues mutated in the cycle (*43*−*45*). We have applied this method of dissecting the energetics of pairwise interactions in protein−protein interfaces to the HyHEL-63/HEL complex. Thus, HyHEL-63 residue A and HEL residue B were mutated (i.e., A → A′, B → B′) separately and together to construct the cycle:

$$\begin{array}{ccc} \text{HyHEL-63(A)HEL(B')} & \rightarrow & \text{HyHEL-63(A')HEL(B')} \\ \uparrow & & \uparrow \\ \text{HyHEL-63(A)HEL(B)} & \rightarrow & \text{HyHEL-63(A')HEL(B)} \end{array}$$

The coupling, or interaction, energy between residues A and B ($\Delta\Delta G_{int}$) is then given by

$$\Delta\Delta G_{int} = -\Delta\Delta G_{AB\rightarrow A'B'} + \Delta\Delta G_{AB\rightarrow A'B} + \Delta\Delta G_{AB\rightarrow AB'} \quad (1)$$

If $\Delta\Delta G_{int}$ equals zero, the effects of the two mutations are independent of each other and the two residues are not coupled. A $\Delta\Delta G_{int}$ other than zero indicates that residues A and B are coupled, either directly or indirectly, since the change in free energy for the association of the double mutant complex is different from the sum of those for the two single mutant complexes.

Double mutant cycles were constructed for 13 amino acid pairs in the HyHEL-63/HEL interface in order to map the interaction energies at the contact surfaces between the proteins (Table 2, Section C). Of the 13 pairs tested, 11 have interacting side chains as judged from the crystal structure, 1 does not form direct contacts but is in proximity (4.6 Å), and 1 is far apart (8.3 Å). Coupling energies were calculated according to eq 1 and are given in Table 3. The interaction between HyHEL-63 V_LAsn32 and $Lys96_{HEL}$ has the largest $\Delta\Delta G_{int}$ (4.4 kcal/mol), in agreement with results from single mutant experiments identifying these residues as hot spots (Figure 2). The residues form a buried hydrogen bond (V_LAsn32 Oδ−Nζ $Lys96_{HEL}$) with good geometry in the crystal structure (Figure 3A). Our $\Delta\Delta G_{int}$ value for this residue pair is consistent with studies showing that deletion of hydrogen bonds involving charged-neutral pairs in the interiors of proteins decreases their stability by 3−5 kcal/mol (*46*). It also agrees remarkably well with a coupling energy of 4.3 kcal/mol for a buried hydrogen bond formed by a charged-neutral pair in the D1.3/E5.2 idiotope−antiidiotope complex (*15*).

Buried salt bridges are generally believed to destabilize folded proteins due to the high desolvation cost associated with transferring charged side chains from the solvent to the protein core (*4*, *47*−*49*). In contrast to protein folding, it has been postulated that salt bridges across a binding interface can, in some cases, significantly stabilize protein−protein

Table 3: Coupling Energies between the Indicated Amino Acid Pairs in the HyHEL-63/HEL Complex as Measured by Double Mutant Cycles[a]

HyHEL-63	HEL	$\Delta\Delta G_{int}$ (kcal/mol)	number and type of side chain−side chain interactions lost in double mutant
V_LN32	K96	4.4	1 buried hydrogen bond and 3 van der Waals contacts
V_LS91	R21	−0.5	no direct contacts, 8.3 Å apart
V_LS91	Y20	1.1	no direct contacts, 4.6 Å apart
V_LY96	R21	−1.1	1 hydrogen bond, partially buried
V_LY96	S100	1.0	1 van der Waals contact
V_HD32	K97	3.0	1 salt bridge and 2 van der Waals contacts
V_HY53	W62	0.7	1 van der Waals contact
V_HY53	W63	0.3	3 van der Waals contacts
V_HY53	L75	1.5	2 van der Waals contacts
V_HY53	D101	−0.2	12 van der Waals contacts
V_HW98	S100	0.4	2 van der Waals contacts
V_HW98	K97	1.8	8 van der Waals contacts
V_HW98	Y20	3.1	1 van der Waals contact

[a] Coupling energies are defined as $\Delta\Delta G_{int} = \Delta\Delta G_{AB\rightarrow A'B} + \Delta\Delta G_{AB\rightarrow AB'} - \Delta\Delta G_{AB\rightarrow A'B'}$, where A and B represent wild-type residues and A′ and B′ represent the mutated residues. Intermolecular contacts were defined by atom pair distances (in Å) less than or equal to the following: C−C, 4.1; C−N, 3.8; C−O, 3.7; N−N, 3.4; N−O, 3.4; O−O, 3.3.

complexes since, after binding, the charged groups may be buried in an environment whose residual composition may be much more hydrophilic than the one after folding (*4*, *50*). Indeed, the interaction between HyHEL-63 V_HAsp32 and Lys97$_{HEL}$, which form the only salt bridge in the complex, has a $\Delta\Delta G_{int}$ of 3.0 kcal/mol, consistent with the identification of Lys97$_{HEL}$ as a hot spot residue by single mutant analysis (Table 2, section A). Although this salt bridge is buried in the interface, it is surrounded by several hydrophilic HEL residues (Asn77, Asn93, Lys96, Ser100, Asp101), which may effectively "solvate" the charged groups forming the salt bridge, thereby increasing its net contribution to complex stabilization. In agreement with this result, $\Delta\Delta G_{int}$ values of similar magnitude have been measured for buried salt bridges in other protein−protein, including antigen−antibody, complexes (*30*, *34*, *51*). In each case, the salt bridge appears to be stabilized by a network of ionic or hydrogen bonding interactions involving adjacent interfacial polar residues. By contrast, a similar analysis of buried salt bridges in the complex between TEM-1 β-lactamase and its protein inhibitor, BLIP, yielded interaction energies of only 1−1.5 kcal/mol (*52*). These differences underscore the apparent influence of local environment on the magnitude of coupling energies for even the same type of interaction. Recently, protein−protein interfaces have been described that are dominated by bridging salt links (*53*, *54*). The energetic contribution of salt bridges in such highly charged interfaces, which are strikingly different from those of other protein−protein complexes of known structure, remains to be evaluated.

No correlation is observed between number of van der Waals contacts and coupling energies for the residue pairs tested. For example, $\Delta\Delta G_{int}$ for the interaction between V_HTyr53 and Asp101$_{HEL}$ is effectively zero (−0.2 kcal/mol), based on the experimental error of our measurement (±0.5 kcal/mol), despite the loss of 12 van der Waals contacts (Table 3). Since both residues are located at the periphery of the interface (Figure 2), the loss of complementarity at this solvent-accessible site may be compensated by local rearrangements in solvent structure, including the incorporation of bound waters in place of the truncated side chains. If so, this suggests that the strength of van der Waals interactions between protein atoms within the V_HTyr53-Asp101$_{HEL}$ residue pair is comparable to that between the protein atoms and water, such that the protein−protein contacts make little or no net contribution to complex stabilization. At the other extreme, a $\Delta\Delta G_{int}$ value of 3.1 kcal/mol was measured between V_HTrp98 and Tyr20$_{HEL}$, in which only a single van der Waals contact is lost in the double mutant (Table 3). Most likely, this large coupling energy is dominated by hydrophobic interactions arising from the burial of two aromatic residues near the center of the interface, isolated from bulk solvent.

Residues V_LTrp96 and Arg21$_{HEL}$ display a negative coupling energy of −1.1 kcal/mol, indicating that the interaction between them destabilizes the HyHEL-63/HEL complex. Superposition of free HEL in three crystal forms (*39*−*41*) onto bound HEL in the HyHEL−63/HEL complex (*13*) reveals significant differences in the conformation the Arg21$_{HEL}$ side chain (not shown). Thus, the entropic cost of "freezing" this flexible side chain in the complex may exceed the energy gained from formation of a long (3.3 Å) hydrogen bond that is partially exposed to solvent.

Double mutant cycles were also constructed for two residue pairs not involved in direct interactions in the crystal structure: V_LSer91−Tyr20$_{HEL}$ and V_LSer91−Arg21$_{HEL}$. While $\Delta\Delta G_{int}$ for the V_LSer91−Arg21$_{HEL}$ pair (−0.5 kcal/mol) is only slightly greater than experimental error, $\Delta\Delta G_{int}$ for the V_LSer91−Tyr20$_{HEL}$ pair (1.1 kcal/mol) equals or exceeds the coupling energies for 6 of the 11 residue pairs tested that form direct contacts across the binding interface (Table 3). It may result from secondary interactions through adjacent residues, such as V_LAsn32, that contact both V_LSer91 and Tyr20$_{HEL}$ in the complex.

CONCLUSIONS

The HyHEL-63/HEL complex may be viewed in the context of other protein−protein complexes that have been similarly analyzed in order to draw some general conclusions concerning the nature of hot spots and the interpretation of mutagenesis data. Bogan and Thorn (*1*) noted that hot spot residues identified by alanine-scanning mutagenesis tend to cluster at the center of interfaces, as in the HyHEL-63/HEL complex, although a number of exceptions have been documented (*7*−*10*, *16*). This observation led to the proposal (the O-ring hypothesis) that occlusion of bulk solvent is, in most cases, a necessary condition for residues to be in hot spots (*1*). According to this hypothesis, the O-ring formed by peripheral residues generates suitable dielectric and solvation conditions for hot spots of interaction energy. Indeed, a lower effective dielectric, which may exist at the center of protein−protein interfaces compared to the periphery, is believed to increase the strength of hydrogen bonds, while the effective hydrophobicity of central residues may be significantly greater than that of peripheral ones (*55*, *56*). However, the possibility also exists that the functional distinction between central and peripheral residues observed in mutagenesis studies simply indicates that side-chain atoms

on the periphery are more easily replaced by water in a nondisruptive manner than atoms at the center of binding interfaces (*6*, *38*). Consistent with this idea, X-ray crystallographic analysis of HEL mutants in complex with antibody D1.3, and of D1.3 mutants bound to HEL, have clearly shown that extensive water-mediated interactions at solvent-accessible sites on the periphery may replace direct hydrogen bonds with little or no loss of binding affinity (*16*, *35*). Moreover, we fail to observe such compensating interactions at the center of the HyHEL-63/HEL interface, where bound waters only partially occupy cavities created by side chain truncations, replacing only a few of the direct protein−protein interactions lost upon mutagenesis (Figure 3). Double mutant cycles, where interactions between amino acids are treated within their native context, represent an improved method for dissecting binding energetics (*43*−*45*). Importantly, HyHEL-63 and HEL residues identified as hot spots by single mutant analysis were also found to make critical interactions in double mutant cycles. However, it must be noted that even interaction energies derived from double mutant cycles may include, in addition to direct interaction energies, indirect effects arising from neighboring residues, conformational changes, and solvent rearrangements (*52*, *57*).

Recently, several more sophisticated approaches have been described for probing hot spots and measuring interaction energies in protein−protein interfaces. Instead of only analyzing individual interactions, Schreiber and colleagues (*52*) examined binding units composed of the interacting residues and their neighbors to estimate the strength of hydrogen bonds in the TEM-1 β-lactamase/BLIP interface. A complex in which all side chains in the binding unit were replaced by alanine was taken as a reference state to which combinations of side chains were introduced. After using double mutant cycles to determine interaction energies for residue pairs in the absence of neighbors, the addition of neighboring residues allowed the evaluation of their cooperative effects on the interactions. We took advantage of the relative accommodation of mutations of hot spot residue V_LTrp92 of D1.3 to estimate the magnitude of the hydrophobic effect in the D1.3/HEL interface (*36*). By replacing V_LTrp92 with residues bearing increasingly smaller side chains and determining the crystal structures and thermodynamic binding parameters for each of the resulting mutant complexes, we demonstrated a correlation between binding free energy and apolar buried surface area that corresponds to 21 cal/mol/Å^2, in excellent agreement with transfer free energy values for small hydrophobic solutes, but lower than the hydrophobic stabilization energy for protein folding. The thermodynamic map of the HyHEL-63/HEL interface described here provides the necessary framework for the application of these, and related (*58*−*60*), methodologies to this system to further our understanding of how structural features contribute to the affinity and specificity of protein−protein association reactions.

REFERENCES

1. Bogan, A. A., and Thorn, K. S. (1998) *J. Mol. Biol. 280*, 1−9.
2. Lo Conte, L., Chothia, C., and Janin, J. (1999) *J. Mol. Biol. 285*, 2177−2198.
3. Sundberg, E. J., and Mariuzza, R. A. (2000) *Structure 8*, 137−142.
4. Sheinerman, F. B., Norel, R., and Honig, B. (2000) *Curr. Opin. Struct. Biol. 10*, 153−159.
5. Ma, B., Wolfson, H. J., and Nussinov, R. (2001) *Curr. Opin. Struct. Biol. 11*, 364−369.
6. DeLano, W. L. (2002) *Curr. Opin. Struct. Biol. 12*, 14−20.
7. Sundberg, E. J., and Mariuzza, R. A. (2002) *Adv. Protein Chem. 61*, 119−160.
8. Dall'Acqua, W., Goldman, E. R., Eisenstein, E., and Mariuzza, R. A. (1996) *Biochemistry 35*, 9667−9676.
9. Leder, L., Llera, A., Lavoie, P. M., Lebedeva, M. I., Li, H.-M., Sékaly, R.-P., Bohach, G. A., Gahr, P. J., Schlievert, P. M., Karjalainen, K., and Mariuzza, R. A. (1998) *J. Exp. Med. 187*, 823−833.
10. Manning, T. C., Schlueter, C. J., Brodnicki, T. C., Parke, E. A., Speir, J. A., Garcia, K. C., Teyton, L., Wilson, I. A., and Kranz, D. M. (1998) *Immunity 8*, 413−425.
11. Clackson, T., and Wells, J. A. (1995) *Science 267*, 383−386.
12. Shapiro, R., Ruiz-Gutierrez, and Chen, C. Z. (2000) *J. Mol. Biol. 302*, 497−519.
13. Li, Y., Li, H., Smith-Gill, S. J., and Mariuzza. R. A. (2000) *Biochemistry 39*, 6296−6309.
14. Li, Y., Grivel, J.-C., Visiwanathan, M., Srinivasan, M., and Smith-Gill, S. J. (1997) *FASEB J. 11*, A1043.
15. Goldman, E. R., Dall'Acqua, W., Braden, B. C., and Mariuzza, R. A. (1997) *Biochemistry 36*, 49−56.
16. Dall'Acqua, W., Goldman, E. R., Lin, W., Teng, C., Tsuchiya, D., Li, H., Ysern, X., Braden, B. C., Li, Y., Smith-Gill, S. J., and Mariuzza, R. A. (1998) *Biochemistry 37*, 7981−7991.
17. Otwinowski, Z., and Minor, W. (1997) *Methods Enzymol. 276*, 307−326.
18. Collaborative Computational Project No. 4 (1994) *Acta Crystallogr. D50*, 760−763.
19. Navaza, J. (1994) *Acta Crystallogr. A50*, 157−163.
20. Brunger, A. T. (1992) *X-PLOR Version 3.1. A System for X-ray Crystallography and NMR*, Yale University Press, New Haven, CT.
21. Brunger, A. T., Adams, P. D., Clore, G. M., DeLano, W. L., Gros, P., Grosse-Kunstleve, R. W., Jiang, J.-S., Kuszewski, J., Nilges, M., Pannu, N. S., Read, R. J., Rice, L. M., Simonson, T., and Warren, G. L. (1998) *Acta Crystallogr. D54*, 905−921.
22. Roussel, A., and Cambillau, C. (1989) TURBO−FRODO. In *Silicon Graphics Geometry Partners Directory*, pp 77−78, Silicon Graphics, Mountain View, CA.
23. Pluckthun, A. (1992) *Immunol. Rev. 130*, 151−188.
24. Wall, J. G., and Pluckthun A. (1995) *Curr. Opin. Biotechnol. 6*, 507−16.
25. Ward, E. S. (1992) *J. Mol. Biol. 224*, 885−888.
26. Wulfing, C., and Pluckthun, A. (1994) *J. Mol. Biol. 242*, 655−669.
27. Granzow, R., and Reed, R. (1992) *Bio/Technology 10*, 390−393.
28. Rajpal, A., and Kirsch, J. F. (1998) *Protein Sci. 7*, 1868−1874.
29. Padlan, E. A., Silverton, E. W., Sheriff, S., Cohen, G. H., Smith-Gill, S. J., and Davies, D. R. (1989) *Proc. Natl. Acad. Sci. U.S.A. 86*, 5938−5942.
30. Pons, J., Rajpal, A., and Kirsch, J. F. (1999) *Protein Sci. 8*, 958−968.
31. Wells, J. A., and de Vos, A. M. (1996) *Annu. Rev. Biochem. 65*, 609−634.
32. Atwell, S., Ultsch, M., and Kossiakoff, A. A. (1997) *Science 278*, 1125−1128.
33. Clackson, M. H., Ultsch, Wells, J. A., and de Vos, A. M. (1998) *J. Mol. Biol. 277*, 1111−1128.
34. Schreiber, G., and Fersht, A. R. (1995) *J. Mol. Biol. 248*, 478−486.
35. Fields, B. A., Goldbaum, F. A., Dall'Acqua, W., Malchiodi, E. L., Cauerhff, A., Schwarz, F. P., Ysern, X., Poljak, R. J., and Mariuzza, R. A. (1996) *Biochemistry 35*, 15494−15503.
36. Sundberg, E. J., Urrutia, M., Braden, B. C., Isern, J., Tsuchiya, D., Fields, B. A., Malchiodi, E. L., Tormo, J., Schwarz, F. P., and Mariuzza, R. A. (2000) *Biochemistry 39*, 15375−15387.
37. Chacko, S., Silverton, E., Kam-Morgan, L., Smith-Gill, S., Cohen, G., and Davies, D. (1995) *J. Mol. Biol. 245*, 261−274.
38. Janin, J. (1999) *Structure 7*, 277−279.
39. Ramanadham, M., Sieker, L. C., and Jensen, L. H. (1990) *Acta Crystallogr. B46*, 63−69.
40. Wilson, K. P., Malcolm, B. A., and Matthews, B. W. (1992) *J. Biol. Chem. 267*, 10842−10849.
41. Madhusudan, Kodandapani, R., and Vijayan, M. (1993) *Acta Crystallogr. D49*, 234−245.
42. Fersht, A. R. (1988) *Biochemistry 27*, 1577−1580.

43. Carter, P. J., Winter, G., Wilkinson, A. J., and Fersht, A. R. (1984) *Cell 38*, 835−840.
44. Ackers, G. K., and Smith, F. R. (1985) *Annu. Rev. Biochem. 54*, 597−629.
45. Horovitz, A. (1987) *J. Mol. Biol. 196*, 733−735.
46. Fersht, A. R., and Serrano, L. (1993) *Curr. Opin. Struct. Biol. 3*, 75−83.
47. Honig, B., and Nicholls, A. (1995) *Science 258*, 1144−1149.
48. Dao-pin, S., Anderson, D. E., Baase, W. A., Dahlquist, F. W., and Matthews, B. W. (1991) *Biochemistry 30*, 11521−11529.
49. Waldburger, C. D., Schildbach, J. F., and Sauer, R. T. (1995) *Nat. Struct. Biol. 2*, 122−128.
50. Xu, D., Lin, S. L., and Nussinov, R. (1997) *J. Mol. Biol. 265*, 68−84.
51. Wibbenmeyer, J. A., Schuck, P., Smith-Gill, S. J., and Willson, R. C. (1999) *J. Biol. Chem. 274*, 26838−26842.
52. Albeck, S., Unger, R., and Schreiber, G. (2000) *J. Mol. Biol. 298*, 503−520.
53. Wang, J. H., Smolyar, A., Tan, K., Lui, J.-H., Kim, M., Sun, Z.-Y. J., Wagner, G., and Reinherz, E. L. (1999) *Cell 97*, 791−803.
54. Tormo, J., Natarajan, K., Margulies, D. H., and Mariuzza, R. A. (1999) *Nature 402*, 623−631.
55. Sharp, K. A., Nicholls, A., Fine, R. M., and Honig, B. (1991) *Science 252*, 106−109.
56. Nicholls, A., Sharp, K. A., and Honig, B. (1991) *Proteins: Struct. Func. Genet. 11*, 281−296.
57. Fersht, A. R., Matouschek, A., and Serrano, L. (1992) *J. Mol. Biol. 224*, 771−782.
58. Wang, W., Lim, W. A., Jakalian, A., Wang, J., Luo, R., Bayly, C., and Kollman, P. A. (2001) *J. Am. Chem. Soc. 123*, 3986−3994.
59. Hodel, M. R., Corbett, A. H., and Hodel, A. E. (2001) *J. Biol. Chem. 276*, 1317−1325.
60. Wang, W., Donini, O., Reyes, C. M., and Kollman, P. A. (2001) *Annu. Rev. Biophys. Biomol. Struct. 30*, 211−243. <

BI020589+